Asian Journal of Chemistry; Vol. 35, No. 12 (2023), 3042-3050

ASIAN JOURNAL OF CHEMISTRY

https://doi.org/10.14233/ajchem.2023.29058

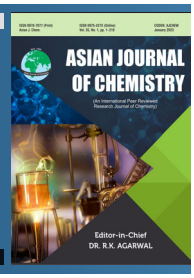

Effective Removal of Selective Heavy Metal Ions from Aqueous Solution through Green Synthesized Zinc Oxide Nanoparticles

KOMAL KASHYAP, MAHESWATA MOHARANA, SONALIKA AGRAWAL, SUBRAT KUMAR PATTANAYAK* and FAHMIDA KHAN*

Department of Chemistry, National Institute of Technology, Raipur-492010, India

*Corresponding authors: E-mail: skpiitbbs@gmail.com; fkhan.chy@nitrr.ac.in

Received: 18 August 2023; *Accepted*: 1 November 2023; *Published online*: 2 December 2023; AJC-21467

In this work, zinc oxide nanoparticles (ZnO NPs) derived from the flower of *Nyctanthus arbor-tristis* have been synthesized in an environmentally benign, safe and non-toxic way. The adsorption of U(VI), Pb(II), Cr(VI) and Cd(II) ions from aqueous solutions by *Nyctanthus arbor-tristis* flower extract was investigated under laboratory conditions to assess its potential in removing these metal ions. The impacts of the experimental factors, such as ZnO NPs dosage, solution pH and contact time, were optimized. The study shows that the majority of the toxic metal ions can be adsorbed from the solution in a relatively short duration of time under ambient conditions. The adsorption behaviour of toxic metal ions onto the ZnO NPs was analyzed with Freundlich as well as Langmuir rate equations and the results were supported by the pseudo-second-order kinetic models. The study provides a safe, non-toxic and eco-friendly green synthesis method and also demonstrated excellent performance of the synthesized ZnO NPs.

Keywords: Zinc oxide nanoparticles, *Nyctanthus arbor-tristis*, Adsorption, Freundlich isotherm, Langmuir isotherm.

INTRODUCTION

Heavy metals have become a significant environmental issue due to their toxicity, ability to accumulate in living organisms and persistence [1]. The primary cause of the rising concern about heavy metals in aquatic environments in recent decades has been the discharge of wastewaters containing heavy metals from a variety of industries, including the production of minerals, petrochemicals, agricultural fertilizers, steel, plastics, tanneries and batteries [2,3]. As heavy metal ions are less biodegradable than organic pollutants, they have the potential to accumulate in the environment and expose living things to high toxicity, leading to hazardous diseases like cancer in humans [4]. In particular, long-term exposure to cadmium damages bones and kidneys, raises blood pressure and promotes the development of cancer [5]. Increase in chromium exposure causes cancer, asthma and diarrhea. Physiological impairment is also caused due to kidney issues, difficulties with the liver and brain defects [6]. The World Health Organization recommendations have established the maximum allowable concentrations of cadmium and chromium in water at 0.003 ppm and 0.05 ppm, respectively [7,8]. Uranium, the most significant radioactive element, is used primarily in nuclear power plants and serves no other significant economic function than that of an energy source. From the perspectives of purification, environment and the disposal of radioactive waste, uranium adsorption onto different solids is highly significant [9]. Therefore, reducing the presence of these heavy metals in aqueous matrices, even in trace amounts, is the main goal of wastewater treatment. The interest in removing these heavy metals from industrial wastewater has increased as a result of recent developments regarding the non-degradability and toxicity of these heavy metals [10]. Therefore, prior to discharge the industrial effluents containing heavy metals into the environment, a pre-treatment technique is necessary.

Several methods including ion-exchange, chemical precipitation, reverse osmosis, membrane processes, microbial biotechnology, coagulation, flocculation, filtration and adsorption technology, have recently been the focus of research studies exploring the removal of heavy metals [11,12]. However, these approaches have a variety of drawbacks, including low efficacy, high costs, the production of harmful byproducts, operational delays, the inability to effectively target particular contaminants and the complexity of the treatment processes [13]. Adsorption

is generally thought to be the most promising strategy due to its great efficacy, cost-effectiveness, flexibility in design and ease of use [14]. In order to address the issue of heavy metal pollution in wastewater, many adsorbents have been prepared to adsorb these metals, which include activated carbon [15], nano adsorbents [16], zeolite [17], chitosan [18] and biochar [19].

Nanoparticles are of great interest to many researchers, due to their remarkable thermal conductivity, exceptional chemical stability, high oxidation potential and environmentally safe manufacturing process [20,21]. The ZnO nanoparticles possesses several advantageous attributes, including wide band-gap, non-toxicity, high binding energy and chemical stability at ambient temperature [22]. The fundamental and easily adjustable properties of ZnO nanoparticles permits its application in a wide range of sectors including biomedicines, wastewater treatment and photoelectronic devices [23-25]. Sol-gel [26], hydrothermal [27] and mechanochemical [28] processes are some examples of the traditional methodologies that can be used to generate nanosized ZnO on a large scale. Despite its application in the commercial sectors, using theses traditional methods reveals a number of limitations. For example, in contrast to the energy-intensive pyrometallurgical process, the chemical method for synthesizing ZnO NPs uses hazardous and damaging chemicals as stabilizers and reductants [29]. Therefore, individuals are interested in finding out some green synthesis processes as a result of increased environmental awareness.

Preparing ZnO NPs from a range of green plant parts, such as roots, leaves, fruit seed, bark and fruit pericarp, is both safe and environmentally beneficial and it also accomplishes the goal of green chemistry [30]. Several bioactive substances, such as amino acids, polyphenolic compounds and carbohydrates are might act as capping agents and affect the production of ZnO NPs [31]. The biological chemicals being natural and biodegradable are less toxic than poisonous chemicals. In present study, the *Nyctanthes arbor-tristis* flower extracts were used for the synthesis of ZnO NPs, which is further used as nanoadsorbent for removing metal contaminants from the water sample. Although the flower extract of *Nyctanthes arbor-tristis* was used for preparing gold nanoparticles [32], however, no studies has been reported on the preparation of ZnO NPs from this plant. Several characterization techniques *viz*. PXRD, FE-SEM, EDS, FTIR and UV Vis spectroscopy confirmed the preparation of ZnO NPs. To study the effects of adsorption capacity of ZnO NPs, different parameters like time, pH, adsorbate concentration as well as absorbent concentration on the absorption of U(VI), Pb (II), Cr(VI) and Cd(II) ions have been studied.

EXPERIMENTAL

Analytical grade zinc acetate dihydrate ($Zn(CH_3COO)_2 \cdot 2H_2O$) obtained from Merck India Pvt. Ltd. Mumbai (India) was used for the synthesis of zinc oxide nanoparticles (ZnO NPs). The flowers of *Nyctanthes arbor-tristis* plant were collected from the campus of National Institute of Technology Raipur, India. The glasswares used in this study were properly rinsed with chromic acid, followed by double-distilled water and dried. All the solutions used in this study were prepared using distilled water.

Preparation of *Nyctanthes arbor-tristis* flower extract: In this work, the *Nyctanthes arbor-tristis* plant extract was prepared by heating 10 g of thorougly washed flowers in 100 mL of distilled water at 60-70 ºC for 2 h in a Tarson's Digital Spinot (spinot™ Digital Magnetic Stirrer and Hot Plate-6040). The stirring was done at 500 rpm under reflux condition. After cooling the reaction mixture to room temperature, it was filtered to obtain a light yellowish brown-coloured liquid extract.

Synthesis of zinc oxide nanoparticles: A 50 mL of zinc acetate dihydrate ($Zn(CH_3COO)_2 \cdot 2H_2O$) solution (0.01 M) was added to the flower extract (50 mL) solution while stirred for 12-24 h using magnetic stirrer. The solution was then cooled to room temperature and allowed to stand for ~30 min. A brown coloured solution was centrifuged at 500 rpm to collect the precipitate, which was further calcined for 1 h at various temperatures to obtain a fine crystalline ZnO nanoparticles.

Characterization: A double beam UV-visible spectroscopy (Model No. LT-2900) was used to obtain the absorption spectra in the range 200 to 600 nm. The FTIR spectra of ZnO NPs were determined by a Fourier transform infrared spectroscope (Agilent Technologies Cary 630) using KBr pellets. The FESEM and EDX techniques were used to study the surface morphology and microstructure properties of synthesized nanoparticles using ZEISS EVO series scanning electron microscope model EVO18). The XRD patterns of ZnO NPs were obtained using an X'Pert Pro X-ray diffractometer (PANalytical 3 kW X'pert powder-multifunctional) with Cu$K\alpha$ as the radiation source at an angle of 10º to 80º.

Analysis of uranium: The batch adsorption activity for U(VI) ion measurement in aqueous water samples using the quantalase LED fluorimeter was assessed. Millipore water was used to make a 5% solution of $Na_4P_2O_7$ and an H_3PO_4 solution was used to keep the pH at 7. This combination functions as a buffer solution (fluorescence enhancer chemical).

Adsorption model and kinetic studies: Both Freundlich and Langmuir adsorption isotherms were studied individually. Impact of contact time was used in the kinetics study. The time variation for the elimination of heavy metal ions throughout the kinetics experiment was conducted from 5 to 140 min, while all other parameters remained constant. The kinetics for four distinct models was done separately with pseudo-first-order, pseudo-second-order, intraparticle diffusion and Elovich kinetic models.

Effect of initial concentration and contact time: A batch adsorption experiment was carried out with 250 mL stoppered flasks (Erlenmeyer flasks) that contain definite volume (100 mL in each flask) of fixed initial concentrations of adsorbates. In order to study the effect of different parameters such as initial concentration, contact time, adsorbent dose, pH and temperature for the removal of U(VI), Pb(II), Cr(VI) and Cd(II) on ZnO NPs. The flasks were agitated using incubator shaker at 200 rpm until equilibrium is reached. The resultant solutions were centrifuged and the supernatant liquids were analyzed by atomic absorption study (AAS) analysis. The amount of adsor-

bate adsorbed at equilibrium condition, q_e (mg/g) was calculated using the following equation:

$$q_e = \frac{q_o - q_t}{W} \times V \quad (1)$$

where q_o and q_e are the initial and equilibrium concentrations (mg/L), respectively; V is the volume of solution and W is the mass of adsorbent used.

The solution of U(VI), Pb(II), Cr(VI) and Cd(II) having concentration of 50 mg/L were used to evaluate the effect of contact time and initial adsorbate concentration on adsorption uptake. For the adsorption of U(VI), Pb(II), Cr(VI) and Cd(II), the adsorbent dose was fixed at 1 mg/L and 100 mg/L (1 to 15 mg/50 mL) accordingly and the solution pH was maintained at 5.5 and 7 unless otherwise stated.

Effect of adsorbent dose: The initial concentration of U(VI), Pb(II), Cr(VI) and Cd(II) solution was 50 mg/L and various amounts of adsorbents (100-500 mg/L) were added to study the effects of adsorbent dosage on these metals. At room temperature, the mixture was agitated until the equilibrium point was attained. Unless otherwise stated, the initial concentration of U(VI), Pb(II), Cr(VI) and Cd(II) solution was maintained at 50 mg/L for all studies.

Effect of pH: In order to investigate effect of pH on the adsorption of U(VI), Pb(II), Cr(VI) and Cd(II), the initial concentrations of 50 mg/L at various pH levels (2.0-10.0) were thoroughly shaked with 2 mg/L of adsorbents. The pH of the solution was maintained using 0.1 N solutions of either NaOH or HCl.

RESULTS AND DISCUSSION

In present study, stable zinc oxide nanoparticles were synthesized in simple steps without chemical stabilizers or surfactants. Furthermore, we successfully synthesized uniform nanoparticles measuring 11.6 nm, which are smaller than ZnO nanoparticles obtained by conventional physical and chemical methods [33-35]. The prepared plant extract acts as a size regulating agent, controlling the aggregation or agglomeration of nanoparticles or crystallites. It also suppresses the nucleation and coalescence of nanoparticles.

Morphological studies: Fig. 1a-b illustrates little agglomeration and predominately hexagonal particle shapes, which is consistent with the reported works [36]. Fig. 1c displays the elemental analysis of the synthesized ZnO NPs as shown in the EDX spectrum, which confirmed their purity and absence of impurities in the sample providing insights into the elemental composition of the synthesized ZnO NPs. The peaks corresponding to zinc and oxygen atoms were observed, but with very low intensities.

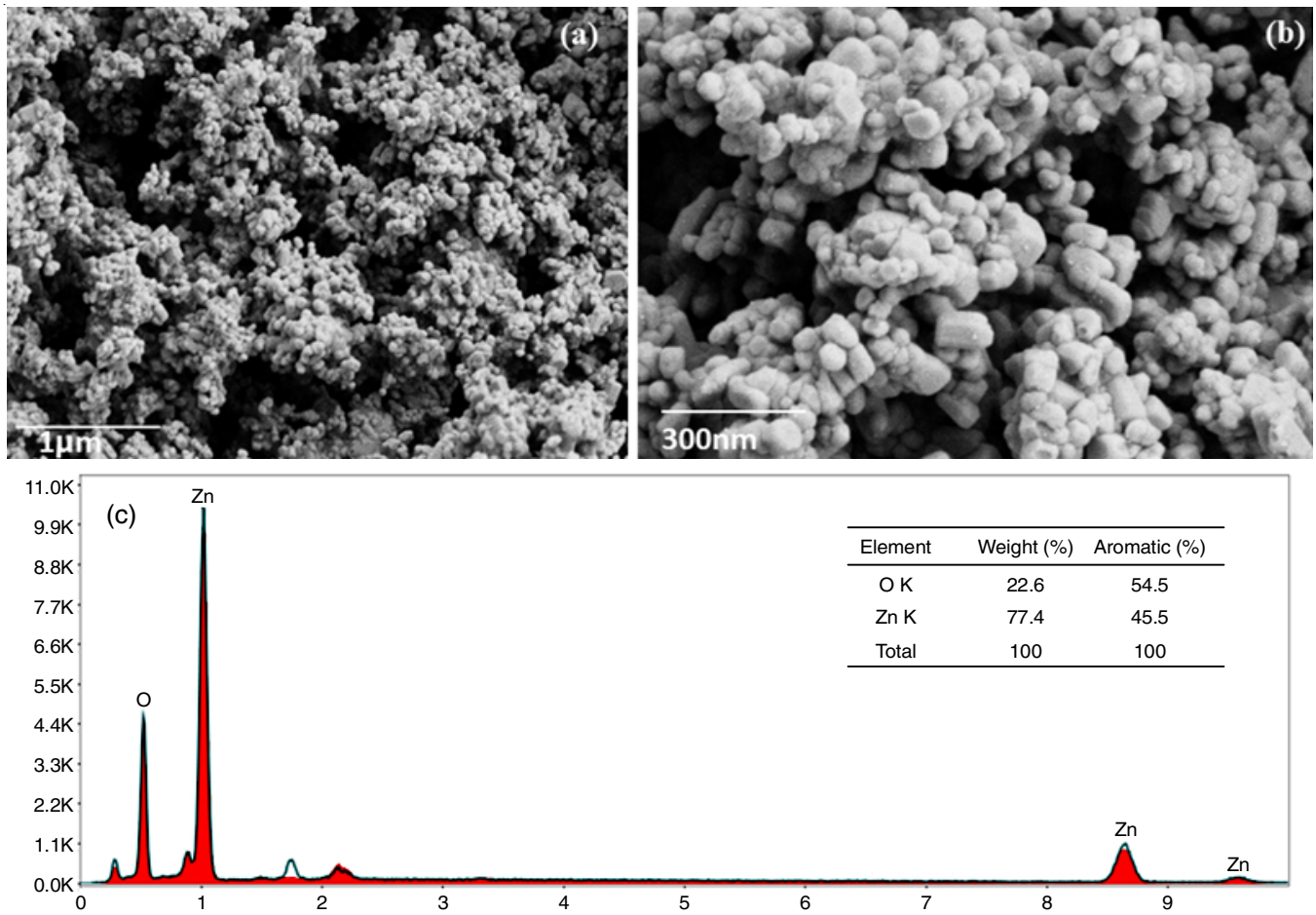

Element	Weight (%)	Aromatic (%)
O K	22.6	54.5
Zn K	77.4	45.5
Total	100	100

Fig. 1. FESEM images of green-synthesized ZnO NPs at different magnification range (a) FESEM at 1 mm range (b) at 300 nm range and (c) EDS analysis of green-synthesized ZnO NPs

FTIR studies: The functional groups present in the plant extract as well as prepared ZnO nanoparticles were identified using FT-IR analysis. The plant extract and ZnO nanoparticles spectra revealed a peak between 3486 and 3286 cm^{-1} due to the –OH stretching vibrations (Fig. 2). The intensity of this vibration decreased after introducing ZnO into cellulose, indicating that the oxygen atom was involved in the bonding interaction with ZnO, resulting in a lowering of the –OH bond strength. A band near 1500 cm^{-1} was attributed to the stretching vibration of C-O group. In any flavonoid compound, the peak at 1435 cm^{-1} is thought to represent a crystallinity band and related to the CH_2 vibration, whereas a band peak about 1000 cm^{-1} was assigned to the stretching vibration of C-O. At 1014 cm^{-1}, there is a small absorption band that represents the stretching vibrations of carboxylic acids.

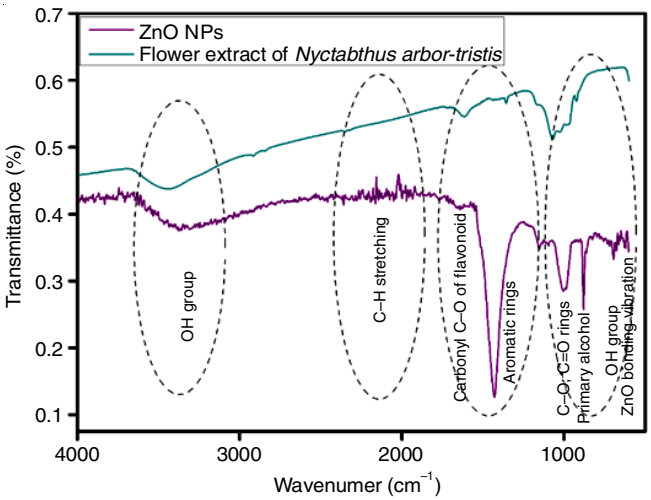

Fig. 2. FTIR spectra of green-synthesized ZnO NPs

XRD studies: The XRD pattern of green-synthesized ZnO NPs has been analyzed at different temperature range (400, 500 and 600 ºC) (Fig. 3). The peaks of ZnO-nanoparticle were observed at 31.91º, 34.56º, 36.39º, 47.68º, 56.74º, 63.04º, 66.58º, 68.11º, 69.20º, 72.68º and 77.12º, which correspondingly correlated to the lattice plane parameters of (100), (002), (101), (200), (102), (110), (103), (200), (112) and (201). The *hkl* planes are matched with the JCPDS card no. 89-7102. The presence of sharp and narrow diffraction peaks suggests the crystalline structure of the peaks. Using Bragg's equation, the interplanar *d*-spacing and its miller indices (*hkl*) were calculated eqn. 2:

$$n\lambda = 2d \sin\theta \quad (2)$$

where n = 1 (order of diffraction), θ = peak position, λ = wavelength of X-ray radiations (1.54 Å), d = interplanar spacing. The average crystallite size of synthesized ZnO and Mg doped ZnO nanoparticles was determined using the Debye-Scherrer's equation [37]:

$$d = \frac{0.89\lambda}{\beta\cos\theta} \quad (3)$$

where β = the FWHM (full width half-maximum) of (101) plane, θ = Bragg's diffraction angle and λ = wavelength of Cu*K*α

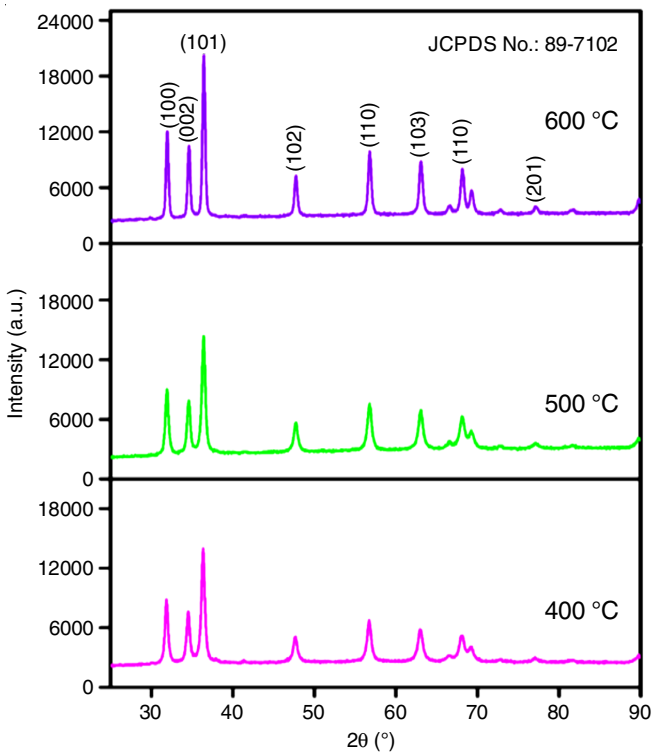

Fig. 3. XRD analysis of green-synthesized ZnO NPs at different temperature

radiation (1.54 Å). According to Debye-Scherrer's equation, the crystallite size of ZnO NPs was found to be 11.6 nm.

UV-visible studies: Absorbance of green-synthesized ZnO NPs was measured by UV-visible spectroscopy at a wavelength between 200 and 800 nm. The peculiar absorption spectra were visible between 330 and 354 nm. Verma *et al.* [38] supported this result by observing that a distinct peak at 329 nm was seen after the reaction mixture's optimization. The analysis of ZnO NPs synthesis involved using surface plasmon resonance (SPR) at a wavelength of 360 nm. This observation revealed that the intrinsic bandgap of ZnO occurs due to the transfer of electrons from the Zn valence band (3*d* orbital) to the O conduction band (2*p* orbital) ($Zn_{3d}O_{2p}$) as shown in Fig. 4.

Using the Tauc relation (eqn. 2), it was determined that the ZnO nanostructure surface's band gap was 2.82 eV, when it absorbed light in the UV absorption at 360 nm. Tauc plot for ZnO NPs is shown in Fig. 4b. The photocatalytic activity of synthesized ZnO NP is restricted to near-UV and visible photoirradiation due to their wide band gap. The determination of optical band gap was done by Tauc's equation [39]:

$$\alpha h\nu = A(h\nu) - (E_g)^{\gamma} \quad (4)$$

where A = absorbance, α = the absorption coefficient represents by α (α = 2.303A/t), t = the cuvette's thickness, ν = photon energy, A = constant. The energy band gap (E_g) for the allowed direct and indirect transition with value n = 1/2 and 2, respectively.

Effect of adsorbent concentration: The removal capacity of ZnO NPs first increases with the solid to liquid mass ratio (Fig. 5) and then increases very slowly until a con-centration of 10 mg. This could be attributed to the fact that when the concentration of the nanoadsorbent increases, the area

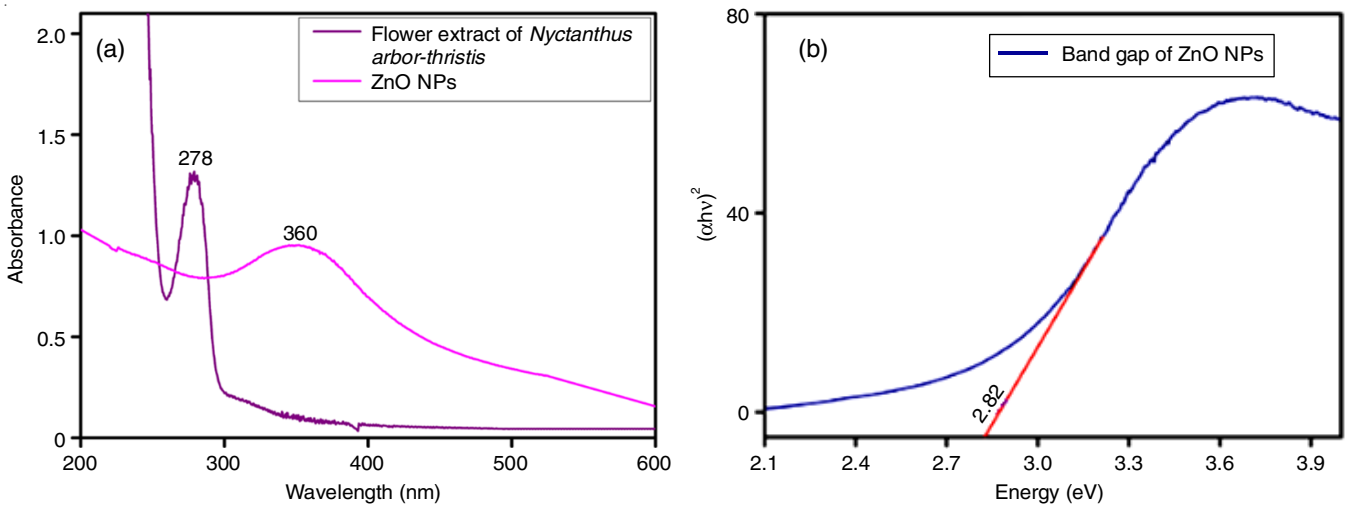

Fig. 4. UV-visible spectra of green-synthesized ZnO NPs (a) UV absorbance of ZnO NPs (b) band gap of prepared ZnO NPs

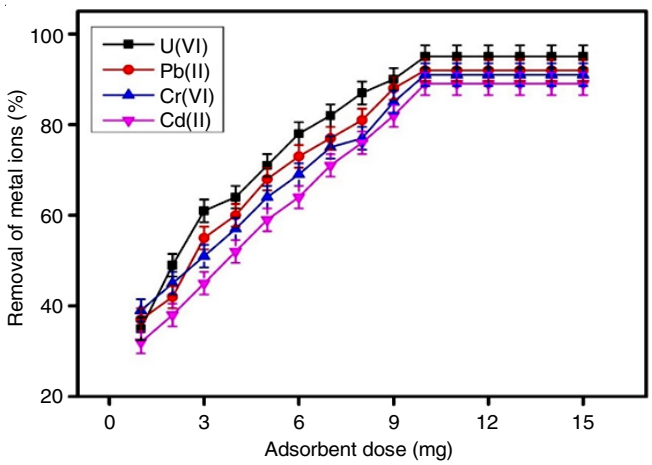

Fig. 5. Effect of adsorbent concentration on adsorption of metal ions by green-synthesized ZnO NPs

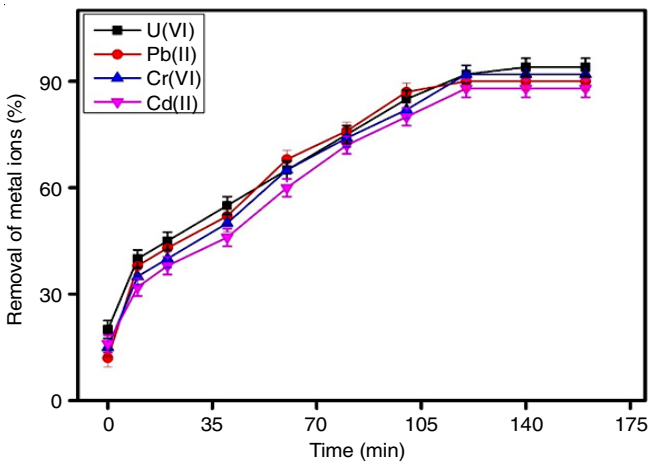

Fig. 6. Effect of contact time on adsorption of metal ions by green-synthesized ZnO NPs

of functional active sites on the surface of the nanomaterial significantly grows, causing the pollutants to be rapidly absorbed from the prepared water samples. As the nanoparticle dosage increases, the efficiency of pollutant absorption will eventually stabilize. The highest percentage of U(VI), Pb(II), Cr(VI) and Cd(II) removal was achieved 95.1%, 91.0%, 89.86% and 87.7%, respectively, while employing a 10 mg dosage of synthesized ZnO NPs.

Effect of contact time: Fig. 6 depicts the effect of contact time interval from of 0 to 140 min. The removal percentage of contaminants increases between 0 and 120 min. The percentage removal then remains constant after that and in some cases, even started to decrease at higher times. The metal ions U(VI), Pb(II), Cr(VI) and Cd(II) may have higher desorption rate from the nanoadsorbent surfaces due to increased contact with the aqueous media. The removal percentage of U(VI), Pb(II), Cr(VI), Cd(II) ions were 94, 90, 92 and 88, respectively at 120 min. The larger surface area as well as high capacity of adsorptive areas on the surfaces of green-synthesized ZnO NPs, which accumulated the organic functional groups produced from plant extract, may be the reason for their increased adsorption properties.

Effect of pH: The ability of ZnO NPs to adsorb toxic metal ions U(VI), Pb(II), Cr(VI), Cd(II) at various pH values between 2 and 10 was investigated (Fig. 7). In this method, 10 mg of ZnO NPs were treated with 50 mL of stock solution of metal ions while holding the other variables constant and being agitated for 2 h at 150 rpm. At pH 4, the removal percentage of 95% and 88% for U(VI) and Cr(VI) ions, respectively was observed, while for Pb(II) and Cd(VI) ions, the removal percentage was found to be 91 and 85%, respectively.

Adsorption studies: To study the removal process at equilibrium, a number of isotherm models, including the Langmuir and Freundlich, are used to examine the contact forces between the holding sites on the surface of nanoadsorbents (ZnO NPs) and the contaiminants [U(VI), Pb(II), Cr(VI) and Cd(II)]. The adsorption capacity of ZnO NPs towards U(VI), Pb (II), Cr(VI) and Cd(II) was examined by applying this model with the classic Langmuir adsorption isotherm as well as Freundlich adsorption isotherm. According to the Langmuir studies, the majority of adsorption takes place on the surface of the adsorbent and there is no adsorbate molecular mobility. The following equation is the mathematical representation of the Langmuir isotherm [40].

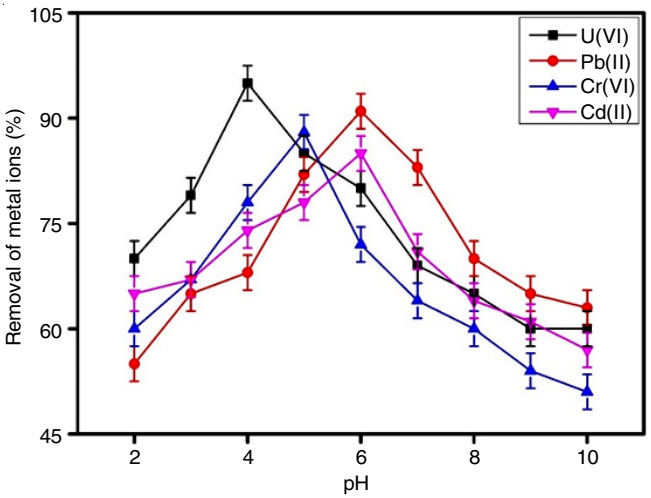

Fig. 7. Effect of pH on adsorption of metal ions by green-synthesized ZnO NPs

$$q_e = \frac{Q_m K_L C_e}{1 + K_L C_e} \quad (5)$$

where Q_m denotes the amount of adsorbed adsorbate on the adsorbent at end point; K_L denotes the Langmuir constant; q_e denotes the amount of adsorbed adsorbate at the equilibrium point; C_e denotes the amount of adsorbate still present at the equilibrium point. The $1/q_e$ *vs.* $1/C_e$ plot is expected to be linear and the above Langmuir isotherm can be written as follows:

$$\frac{1}{q_e} = \frac{1}{Q_m} + \frac{1}{Q_m K_L}\frac{1}{C_e} \quad (6)$$

A key parameter of the Langmuir adsorption isotherm commonly known as the equilibrium parameter (R_L), which can be derived using eqn. 4:

$$R_L = \frac{1}{1 + K_L C_o} \quad (7)$$

where Langmuir constant is denoted by K_L and C_o represent the initial concentration of analyte. If the R_L value is between 0 and 1 favour the Langmuir adsorption, if it is more than 1, it indicates adsorption process is unfavourable.

The Freundlich adsorption isotherm primarily describes the multilayer adsorption in the liquid to solid phase and is represented by eqn. 8:

$$q_e = k_f C_e^{1/n} \quad (8)$$

where the variables q_e and C_e are the same as those in the Langmuir equation, Freundlich constant denoted by k_f and the heterogeneity of the adsorbent's surface is represented by "n" which stands for the Freundlich exponent. The above equation may be rewritten in the simplified form to obtain eqn. 9:

$$\log q_e = \log K_f + \frac{1}{n}\log C_e \quad (9)$$

Table-1 displays the correlation coefficient (R^2) values obtained from the graph, together with the calculated values of all other estimated parameters for the determination of the dimensionless factor (R_L). The R_L values obtained were 0 and 1, indicating the advantageous impact of Langmuir adsorption. The Freundlich adsorption exponent "n" which must be equal to or greater than 1, indicates the presence of more favourable surfaces for adsorption by higher values [41]. Table-2 shows the adsorption capacity data for all ions in a 100 ppm solution.

Kinetic studies: For the removal of U(VI), Pb(II), Cr(VI) and Cd(II) by ZnO NPs, the equilibrium adsorption model was compared to the pseudo-first and pseudo-second orders of Lagergren's kinetic model, intraparticle diffusion model and Elovich model [40,42].

The pseudo first-order-equation is expressed as:

$$\ln(q_e - q_t) = \ln q_e - k_1 t \quad (10)$$

TABLE-1
PFO AND PSO MODELS OF ADSORPTION KINETICS PARAMETERS FOR REMOVAL OF U(VI), Pb(II), Cr(VI) AND Cd(II) METAL IONS BY ZnO NPs

Parameters	U(VI)		Pb(II)		Cr(VI)		Cd(II)	
	PFO	PSO	PFO	PSO	PFO	PSO	PFO	PSO
Intercept	3.55	0.07	3.49	0.30	3.12	0.655	2.84	1.60
Slope	0.0087	0.170	0.041	0.155	0.38	0.14	0.035	0.14
R^2	0.92	0.99	0.97	0.98	0.95	0.98	0.91	0.97
q_e	34.81	5.88	32.78	6.54	22.64	7.14	17.11	7.14
K_1	9.6×10^{-5}	–	4.5×10^{-4}	–	4.2×10^{-4}	–	3.8×10^{-4}	–
K_2	–	0.413	–	0.077	–	0.029	–	0.012

TABLE-2
LANGMUIR AND FREUNDLICH ADSORPTION PARAMETERS FOR REMOVAL OF U(VI), Pb(II), Cr(VI) AND Cd(II) METAL IONS BY ZnO NPs

Parameters	U(VI)		Pb(II)		Cr(VI)		Cd(II)	
	Langmuir	Freundlich	Langmuir	Frendlich	Langmuir	Frendlich	Langmuir	Frendlich
q_{max}	333	–	500	–	200	–	166.67	–
K_1	564.9	–	1020.4	–	434.78	–	320.51	–
n	–	0.87	–	0.880	–	0.89	–	0.90
k_f	–	7.76	–	6.918	–	6.16	–	5.49
R^2	0.96	0.95	0.98	0.960	0.96	0.96	0.95	0.96

$$\frac{1}{q_t} = \frac{t}{q_e} + \frac{1}{k_2 q_e^2} \quad (11)$$

$$q_t = k_i t^{1/2} + C \quad (12)$$

$$q_t = \frac{1}{\beta}\ln(\alpha\beta) + \frac{1}{\beta}\ln t \quad (13)$$

where q_t and q_e indicates the amount of adsorbed adsorbate at equilibrium and at time 't', respectively; k_1 is the rate constant (min^{-1}). The rate constant for pseudo-first order, k_1 (min^{-1}) was derived using the intercept and slope of the line graph log (q_e - q_t) *versus* t (time). The slope and intercept of the linear graph of t/q_t *versus* time (t) were used to calculate the pseudo-second order rate constant k_2 (g mg^{-1} min^{-1}).

Fig. 8 shows the plotted results of the removal kinetic investigations for the intraparticle diffusion model, the pseudo-first order and pseudo-second order and the Elovich kinetic models. Fig. 8a-b exhibits the pseudo first-order and pseudo second-order kinetics, respectively. The equilibrium adsorption data are more acceptable for pseudo second-order models than for pseudo first-order models, according to the kinetic results. These results were further proved by the presence of a high correlation coefficient (> 0.90) and the graph's strong linearity in depicting the relationship between t/q_t and time (t). The kinetic results indicated that the adsorption of U(VI), Pb(II), Cr(VI) and Cd(II) on the surface of ZnO nanoadsorbents is the physio-adsorption process. Table-1 shows the correlation coefficient (R^2) values that were determined using the specified equations for all metal ions at varied concentrations. The pseudo-second-order kinetic model more closely matches the experimental data and R^2 values.

The best-fitting kinetic models on the adsorbent surfaces was selected using the kinetic evaluations of four models and R^2 values. Table-3 shows the correlation coefficients and parameters derived using four different kinetic models.

Comparative studies: The adsorption capacity of ZnO nanoparticles for the removal of U(VI), Pb (II), Cr(VI) and Cd(II) metal ions was compared to other nanoadsorbents, which have been reported in literature and are listed in Table-4. The fact that the adsorbent utilized in this study had a greater adsorption capacity than other reported nanostructure adsorbents suggests that synthesized ZnO NPs from is a promising adsorbent of U(VI), Pb (II), Cr(VI) and Cd(II) metal ions from wastewaters.

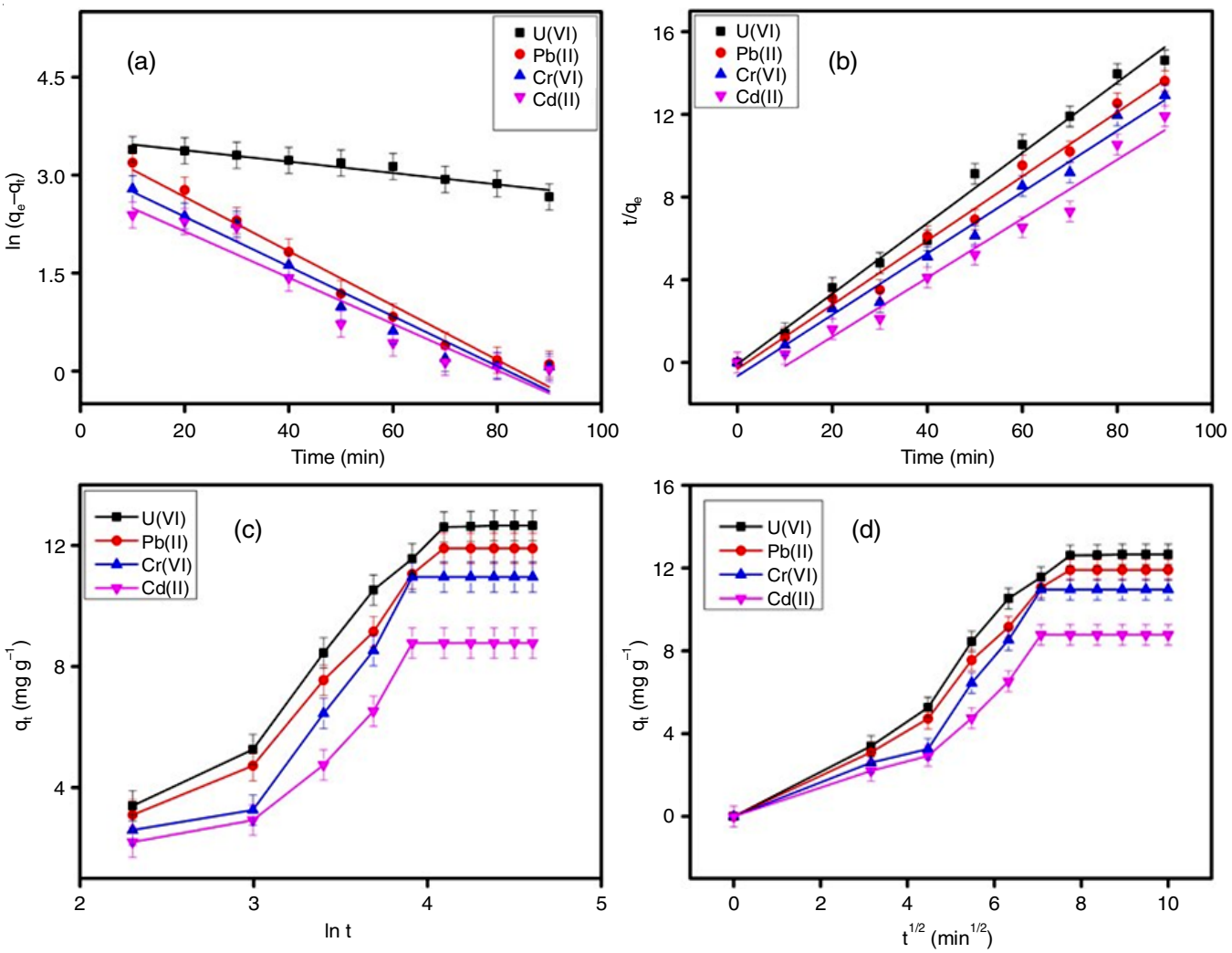

Fig. 8. Adsorption kinetics includes the following: (a) pseudo 1st order kinetics; (b) pseudo 2nd order kinetics; (c) the intraparticle diffusion model; and (d) the Elovich model for removal of U(VI), Pb (II), Cr(VI) and Cd(II)metal ions by ZnO NPs

TABLE-3
INTRAPARTICLE DIFFUSION (IPD) AND ELOVICH MODELS OF ADSORPTION KINETICS PARAMETERS FOR REMOVAL OF HMIs IONS BY ZnO NPs FROM WATER SAMPLES

Parameters	U(VI)		Pb(II)		Cr(VI)		Cd(II)	
	IPD	Elovich	IPD	Elovich	IPD	Elovich	IPD	Elovich
K_{diff}	0.046	–	1.36	–	1.29	–	1.03	–
C	1.43	–	-0.17	–	-0.52	–	-0.40	–
R^2	0.92	0.93	0.92	0.93	0.89	0.88	0.90	0.88
α	–	0.221	–	0.228	–	0.229	–	0.290
β	–	0.96	–	0.843	–	0.119	–	0.564

TABLE-4
COMPARISON RESULT OF PREVIOUSLY REPORTED VARIOUS ADSORBENTS FOR THE REMOVAL OF HEAVY METAL IONS BY ZnO NPs FROM WATER SAMPLES

Adsorbents	Metal ions (M^{n+})	Adsorption capacity (mg/g)	Ref.
ZnO nanoparticles	U(VI)	3.39	[43]
GO-ZnO	U(VI)	476.19	[44]
rGO-ZnO	U(VI)	256.41	[44]
ZnO NPs	U(VI)	333.00	Present work
ZnO nanoparticles	Pb(II)	166.67	[41]
Silver and zinc nanoparticles functionalized cellulose	Pb(II)	43.81	[45]
Zn-Al-NTA composites	Pb(II)	5.814	[46]
ZnO NPs	Pb(II)	500.00	Present work
Zinc oxide nanoparticles	Cr(VI)	88.547	[47]
Zincebiochar from sugarcane bagasse	Cr(VI)	~ 14.00	[48]
H-NZVI	Cr(VI)	40.40	[49]
ZnO NPs	Cr(VI)	200.00	Present work
ZnO nanoparticles	Cd(II)	149.62	[41]
$CuFe_2O_4$ nanoparticles	Cd(II)	17.54	[50]
ZnO	Cd(II)	179.00	[51]
ZnO NPs	Cd(II)	166.67	Present work

Conclusion

Zinc oxide nanoparticles (ZnO NPs) were synthesized by a sustainable and eco-friendly synthetic method utilizing the flower extract of *Nyctanthus arbor-tristisis*. The XRD and FE-SEM were employed to illustrate the crystalline structure of ZnO NPs, which had a nanoscale size range of 11.6 nm. FTIR study revealed that the reduction of zinc metal ions to zinc nanoparticles required the involvement of constituents from the group of bioactive compounds. At pH 4, the removal percentage of U(VI) and Cr(VI) ions shows 95% and 88% similarly at pH 6, whereas Pb(II) and Cd(VI) ion observed to be 91 and 85% respectively. The Langmuir isotherms matched with the the experimental data with R^2 = 0.96, 0.98, 0.96, 0.96 for U(VI), Pb(II), Cr(VI) and Cd(II), respectively. The kinetic studies the pseudo-second-order kinetic model shows best result with value of R^2 = 0.99, 0.98, 0.98, 0.97 for U(VI), Pb(II), Cr(VI) and Cd(II), respectively. These results indicated that zinc oxide nanoparticles synthesized from *Nyctanthus arbor-tristisis* flower extracts are a promising nanoadsorbent for the purification of water.

ACKNOWLEDGEMENTS

One of the authors, Komal Kashyap, expresses her sincere gratitude to the CSIR-UGC NET (File No. [09/1116(0007)/2018/EMR-I]), New Delhi, India for awarded a JRF-SRF fellowship. The authors also acknowledge to Department of Chemistry, National Institute of Technology, Raipur, India for providing research facilities.

CONFLICT OF INTEREST

The authors declare that there is no conflict of interests regarding the publication of this article.

REFERENCES

1. X. Weng, X. Jin, J. Lin, R. Naidu and Z. Chen, *Ecol. Eng.*, **97**, 32 (2016); https://doi.org/10.1016/j.ecoleng.2016.08.003
2. S.M. Ghasemabadi, M. Baghdadi, E. Safari and F. Ghazban, *J. Environ. Chem. Eng.*, **6**, 4840 (2018); https://doi.org/10.1016/j.jece.2018.07.014
3. V.V. Martins, M.O.B. Zanetti, A. Pitondo-Silva and E.G. Stehling, *Environ. Sci. Pollut. Res. Int.*, **21**, 5873 (2014); https://doi.org/10.1007/s11356-014-2509-4
4. Ihsanullah, A. Abbas, A.M. Al-Amer, T. Laoui, M.J. Al-Marri, M.S. Nasser, M. Khraisheh and M.A. Atieh, *Sep. Purif. Technol.*, **157**, 141 (2016); https://doi.org/10.1016/j.seppur.2015.11.039
5. K. Sangeetha, G. Vidhya, G. Vasugi and E.K. Girija, *J. Environ. Chem. Eng.*, **6**, 1118 (2018); https://doi.org/10.1016/j.jece.2018.01.018
6. T.C. Egbosiuba, A.S. Abdulkareem, A.S. Kovo, E.A. Afolabi, J.O. Tijani, M.T. Bankole, S. Bo and W.D. Roos, *Sci. Rep.*, **11**, 75 (2021); https://doi.org/10.1038/s41598-020-79857-z
7. World Health Organization, World Health Statistics, World Health Organization (2010).
8. L. Levankumar, V. Muthukumaran and M.B. Gobinath, *J. Hazard. Mater.*, **161**, 709 (2009); https://doi.org/10.1016/j.jhazmat.2008.04.031

9. C. Kütahyalý and M. Eral, *Sep. Purif. Technol.*, **40**, 109 (2004); https://doi.org/10.1016/j.seppur.2004.01.011
10. Z. Liu, X. Li, P. Zhan, F. Hu and X. Ye, *Sep. Purif. Technol.*, **206**, 199 (2018); https://doi.org/10.1016/j.seppur.2018.06.007
11. S. Mustapha, J.O. Tijani, M.M. Ndamitso, S.A. Abdulkareem, D.T. Shuaib, A.K. Mohammed and A.J.S.R. Sumaila, *Sci. Rep.*, **10**, 13068 (2020); https://doi.org/10.1038/s41598-020-69808-z
12. F. Fu and Q. Wang, *J. Environ. Manage.*, **92**, 407 (2011); https://doi.org/10.1016/j.jenvman.2010.11.011
13. S. Muzaffar and H. Tahir, *J. Mol. Liq.*, **252**, 368 (2018); https://doi.org/10.1016/j.molliq.2018.01.007
14. X. Li, S. Wang, Y. Liu, L. Jiang, B. Song, M. Li, G. Zeng, X. Tan, X. Cai and Y. Ding, *J. Chem. Eng. Data*, **62**, 407 (2017); https://doi.org/10.1021/acs.jced.6b00746
15. S. Parlayici, V. Eskizeybek, A. Avci and E. Pehlivan, *J. Nanostructure Chem.*, **5**, 255 (2015); https://doi.org/10.1007/s40097-015-0156-z
16. A.L. Petranovska, N.V. Abramov, S.P. Turanska, P.P. Gorbyk, A.N. Kaminskiy and N.V. Kusyak, *J. Nanostructure Chem.*, **5**, 275 (2015); https://doi.org/10.1007/s40097-015-0159-9
17. S. Wang and Y. Peng, *Chem. Eng. J.*, **156**, 11 (2010); https://doi.org/10.1016/j.cej.2009.10.029
18. W.S. Wan Ngah, L.C. Teong and M.A.K.M. Hanafiah, *Carbohydr. Polym.*, **83**, 1446 (2011); https://doi.org/10.1016/j.carbpol.2010.11.004
19. X. Tan, Y. Liu, G. Zeng, X. Wang, X. Hu, Y. Gu and Z. Yang, *Chemosphere*, **125**, 70 (2015); https://doi.org/10.1016/j.chemosphere.2014.12.058
20. R. Ranjbarzadeh, A. Moradikazerouni, R. Bakhtiari, A. Asadi and M. Afrand, *J. Clean. Prod.*, **206**, 1089 (2019); https://doi.org/10.1016/j.jclepro.2018.09.205
21. G. Yang, C. Zhu, D. Du, J. Zhu and Y. Lin, *Nanoscale*, **7**, 14217 (2015); https://doi.org/10.1039/C5NR03398E
22. D.E. El-Ghwas, A.S. Al-Nasser and G.A. Zamil, *Res. J. Pharm. Technol.*, **15**, 471 (2022); https://doi.org/10.52711/0974-360X.2022.00077
23. A.D. Terna, E.E. Elemike, J.I. Mbonu, O.E. Osafile and R.O. Ezeani, *Mater. Sci. Eng. B*, **272**, 115363 (2021); https://doi.org/10.1016/j.mseb.2021.115363
24. K.G. Thakre, D.P. Barai and B.A. Bhanvase, *Water Environ. Res.*, **93**, 2414 (2021); https://doi.org/10.1002/wer.1623
25. W. Liu, K. Liu, H. Du, T. Zheng, N. Zhang, T. Xu, B. Pang, X. Zhang, C. Si and K. Zhang, *Nano-Micro Lett.*, **14**, 104 (2022); https://doi.org/10.1007/s40820-022-00849-x
26. I.M. Factori, J.M. Amaral, P.H. Camani, D.S. Rosa, B.A. Lima, M. Brocchi, E.R. da Silva and J.S. Souza, *ACS Appl. Nano Mater.*, **4**, 7371 (2021); https://doi.org/10.1021/acsanm.1c01334
27. M.M. ElFaham, A.M. Mostafa and E.A. Mwafy, *J. Phys. Chem. Solids*, **154**, 110089 (2021); https://doi.org/10.1016/j.jpcs.2021.110089
28. W. Ao, J. Li, H. Yang, X. Zeng and X. Ma, *Powder Technol.*, **168**, 148 (2006); https://doi.org/10.1016/j.powtec.2006.07.014
29. K.K. Brar, S. Magdouli, A. Othmani, J. Ghanei, V. Narisetty, R. Sindhu, P. Binod, A. Pugazhendhi, M.K. Awasthi and A. Pandey, *Environ. Res.*, **207**, 112202 (2022); https://doi.org/10.1016/j.envres.2021.112202
30. R.A. Sheldon, *Chem. Soc. Rev.*, **41**, 1437 (2012); https://doi.org/10.1039/C1CS15219J
31. B. Yuliarto, N.L.W. Septiani, Y.V. Kaneti, M. Iqbal, G. Gumilar, M. Kim, J. Na, K.C.W. Wu and Y. Yamauchi, *New J. Chem.*, **43**, 15846 (2019); https://doi.org/10.1039/C9NJ03311D
32. H. Tabasum, B.A. Bhat, B.A. Sheikh, V.N. Mehta and J.V. Rohit, *Inorg. Chem. Commun.*, **145**, 110015 (2022); https://doi.org/10.1016/j.inoche.2022.110015
33. M.S.E.D. Salem, A.Y. Mahfouz and R.M. Fathy, *Biometals*, **34**, 175 (2021); https://doi.org/10.1007/s10534-020-00271-z
34. J.Z. Kong, A.D. Li, H.F. Zhai, Y.P. Gong, H. Li and D. Wu, *J. Solid State Chem.*, **182**, 2061 (2009); https://doi.org/10.1016/j.jssc.2009.03.022
35. W. Wanas, S.A. Abd El-Kareem, S. Ebrahim, M. Soliman and M. Karim, *Sci. Rep.*, **13**, 27 (2023); https://doi.org/10.1038/s41598-022-27111-z
36. C. Jayaseelan, A.A. Rahuman, A.V. Kirthi, S. Marimuthu, K. Gaurav, T. Santhoshkumar, A. Bagavan, L. Karthik and K.B. Rao, *Spectrochim. Acta A Mol. Biomol. Spectrosc.*, **90**, 78 (2012); https://doi.org/10.1016/j.saa.2012.01.006
37. H.M. Xiong, D.G. Shchukin, H. Möhwald, Y. Xu and Y.Y. Xia, *Angew. Chem. Int. Ed.*, **48**, 2727 (2009); https://doi.org/10.1002/anie.200805590
38. P.R. Verma, F. Khan and S. Banerjee, *Inorg. Nano-Metal Chem.*, **51**, 427 (2020); https://doi.org/10.1080/24701556.2020.1793355
39. P. Ramesh, K. Saravanan, P. Manogar, J. Johnson, E. Vinoth and M. Mayakannan, *Sens. Biosensing Res.*, **31**, 100399 (2021); https://doi.org/10.1016/j.sbsr.2021.100399
40. Y. Jia, L. Ding, P. Ren, M. Zhong, J. Ma and X. Fan, *J. Chem. Eng. Data*, **65**, 725 (2020); https://doi.org/10.1021/acs.jced.9b00951
41. A. Radhakrishnan, P. Rejani, J.S. Khan and B. Beena, *Ecotoxicol. Environ. Saf.*, **133**, 457 (2016); https://doi.org/10.1016/j.ecoenv.2016.08.001
42. S.I. Ali, S.M. Lalji, Z. Awan, S. Hashmi, G. Khan and M. Asad, *Chem. Zvesti*, **77**, 1017 (2023); https://doi.org/10.1007/s11696-022-02539-9
43. A. Radhakrishnan, J. Nahi and B. Beena, *Mater. Today Proc.*, **41**, 557 (2021); https://doi.org/10.1016/j.matpr.2020.05.249
44. I.G. Kaptanoglu and S. Yusan, *J. Radioanal. Nucl. Chem.*, **332**, 4705 (2023); https://doi.org/10.1007/s10967-023-08876-7
45. A.A. Badawy, A.F. Ghanem, M.A. Yassin, A.M. Youssef and M.H. Abdel Rehim, *Environ. Nanotechnol. Monit. Manag.*, **16**, 100501 (2021); https://doi.org/10.1016/j.enmm.2021.100501
46. R.M.A.Q. Jamhour, T.S. Ababneh, A.I. Al-Rawashdeh, G.M. Al-Mazaideh, T.M.A. Al Shboul and T.M. Jazzazi, *Adv. Anal. Chem.*, **6**, 17 (2016).
47. M. Gu, L. Hao, Y. Wang, X. Li, Y. Chen, W. Li and L. Jiang, *Chem. Phys.*, **534**, 110750 (2020); https://doi.org/10.1016/j.chemphys.2020.110750
48. C. Gan, Y. Liu, X. Tan, S. Wang, G. Zeng, B. Zheng, T. Li, Z. Jiang and W. Liu, *RSC Adv.*, **5**, 35107 (2015); https://doi.org/10.1039/C5RA04416B
49. R. Fu, X. Zhang, Z. Xu, X. Guo, D. Bi and W. Zhang, *Sep. Purif. Technol.*, **174**, 362 (2017); https://doi.org/10.1016/j.seppur.2016.10.058
50. Y.J. Tu, C.F. You and C.K. Chang, *J. Hazard. Mater.*, **235-236**, 116 (2012); https://doi.org/10.1016/j.jhazmat.2012.07.030
51. L. Khezami, K.K. Taha, E. Amami, Ghiloufi and L. El Mir, *Desalination Water Treat.*, **62**, 346 (2017); https://doi.org/10.5004/dwt.2017.0196